Anodic-oxide-induced interdiffusion in GaAs/AlGaAs quantum wells

Shu Yuan,[a] Yong Kim,[b] H. H. Tan, and C. Jagadish[c]
Department of Electronic Materials Engineering, Research School of Physical Sciences and Engineering, The Australian National University, Canberra, ACT 0200, Australia

P. T. Burke, L. V. Dao, and M. Gal
School of Physics, University of New South Wales, Sydney, NSW 2052, Australia

M. C. Y. Chan and E. H. Li
Department of Electrical and Electronic Engineering, University of Hong Kong, Pokfulam Road, Hong Kong

J. Zou, D. Q. Cai, and D. J. H. Cockayne
Electron Microscope Unit and Australian Key Center for Microscopy and Microanalysis, The University of Sydney, NSW 2006, Australia

R. M. Cohen
Department of Materials Science and Engineering, University of Utah, Salt Lake City, Utah 84112

(Received 28 April 1997; accepted for publication 22 October 1997)

Enhancement of interdiffusion in GaAs/AlGaAs quantum wells due to anodic oxides was studied. Photoluminescence, transmission electron microscopy, and quantum well modeling were used to understand the effects of intermixing on the quantum well shape. Residual water in the oxide was found to increase the intermixing, though it was not the prime cause for intermixing. Injection of defects such as group III vacancies or interstitials was considered to be a driving force for the intermixing. Different current densities used in the experimental range to create anodic oxides had little effect on the intermixing. © *1998 American Institute of Physics.* [S0021-8979(98)04103-6]

I. INTRODUCTION

Interdiffusion in quantum wells (QW) has recently attracted much interest in device applications and physics,[1–3] since it can be used to modify materials and device properties. Interdiffusion between QW and adjacent barriers results in a change of the QW shape which in turn modifies the subband energies in the conduction band and the valence band.[4] This property can be used to postgrowth modify the lasing wavelength of quantum well lasers and the absorption coefficient of waveguides and photodetectors, it can also be used to improve lateral carrier confinement of ridge waveguide lasers. As refractive index is directly related to absorption coefficient,[5] interdiffusion also modifies the refractive index.[6–8] This can be used to improve lateral optical confinement and thus side-mode suppression in quantum well lasers and to fabricate waveguides. Interdiffusion has been applied to the fabrication of high-reliability blue-shifted InGaAsP/InP,[9] GaAs/AlGaAs,[10] and InGaAs–GaAs[11] lasers. It has been applied to improve the performance of high-speed lasers,[12] multiple wavelength lasers,[13,14] low-threshold current lasers,[15] lasers with saturable absorbers.[16] Output power of high power quantum well lasers was considerably increased after fabrication of nonabsorbing mirrors using interdiffusion.[17] Monolithic integration of various optoelectronic devices like lasers, modulators, wavelength division multiplexing sources, and waveguides can be achieved by selective area quantum well intermixing.[18–20] It has been predicted that interdiffusion will enhance the side-mode suppression ratio in $\lambda/4$ shifted distributed feedback lasers[21] and enhance the absorption strength and responsivity of infrared photodetectors.[22]

There are two kinds of interdiffusion techniques used widely, one is the impurity-induced interdiffusion,[2,23–26] another is the impurity-free interdiffusion.[27,28] The impurity-induced interdiffusion usually introduces substantial undesired changes in the material resistivity and trap concentrations. The case of impurity-free interdiffusion can create large band gap energy shifts without such problems associated with impurity-induced interdiffusion. Recently, photoabsorption-induced interdiffusion, i.e., laser intermixing, has been developed mainly for use in the InGaAsP system.[18] In the GaAs/AlGaAs system, SiO_2 and Si_3N_4 are commonly used to promote and prevent interdiffusion, respectively. SiO_2, however, reacts with Al when in direct contact with AlGaAs, and thus generates Si which behaves as an impurity source. Si_3N_4, on the other hand, causes considerable strain.[3,29]

Recently we have demonstrated a novel impurity-free interdiffusion in GaAs/AlGaAs system,[30] namely anodic-oxide-induced interdiffusion. A portion of the GaAs cap layer of the GaAs/AlGaAs quantum well structure is anodically oxidized, the oxide enhances the interdiffusion at high temperature. We have recently applied this technique to observe the photoluminescence (PL) and cathodoluminescence signals from *V*-grooved quantum wires and obtained both spectrally and spatially well-resolved light emission from quantum wires both at low temperature and room temperature.[31] Pulsed anodic oxide is used as the cap to promote interdiffusion in quantum wells beneath the cap. The

[a]Electronic mail: shu.yuan@anu.edu.au
[b]Present address: Semiconductor Materials Research Center, Korea Institute of Sciences and Technology, P.O. Box 131, Cheongryang, Seoul, Korea.
[c]Electronic mail: cxj109@rsphysse.anu.edu.au

TABLE I. Samples structure. All epilayers are nominally undoped and grown on the P^+GaAs substrates by low pressure MOCVD.

Sample A		Sample B	
GaAs	300 nm	GaAs	100 nm
$Al_{0.3}Ga_{0.7}As$	50 nm	$Al_{0.54}Ga_{0.46}As$	50 nm
GaAs (QW)	3.2 nm	GaAs (QW4)	1.3 nm
$Al_{0.3}Ga_{0.7}As$	50 nm	$Al_{0.54}Ga_{0.46}As$	50 nm
GaAs (buffer)	500 nm	GaAs (QW3)	2.9 nm
P^+GaAs	substrate	$Al_{0.54}Ga_{0.46}As$	50 nm
		GaAs (QW2)	3.7 nm
		$Al_{0.54}Ga_{0.46}As$	50 nm
		GaAs (QW1)	8.6 nm
		$Al_{0.54}Ga_{0.46}As$	50 nm
		GaAs (buffer)	500 nm
		P^+GaAs	substrate

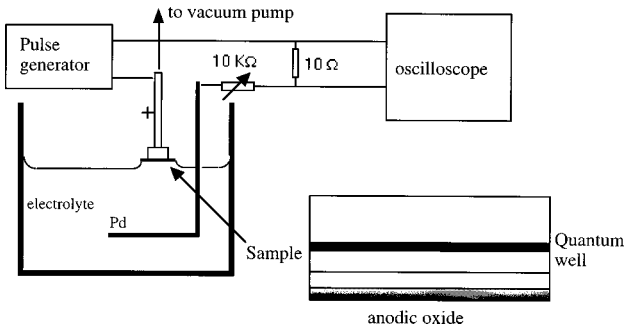

FIG. 1. Schematic diagram showing the anodic oxidization setup used in this work. The electrolyte is composed of ethylene glycol, deionized water, and phosphoric acid (40:20:1 by volume).

pulsed anodization technique[32] has recently attracted attention as a new way of creating current blocking layers for ridge-waveguide quantum well laser fabrication, since it is simple, reliable, and cost effective.[33–36] The anodic-oxide-induced interdiffusion is very simple: the anodization is done at room temperature for a few minutes without special sample preparation, the rapid thermal annealing (RTA) is done in a flowing inert gas. Selective area interdiffusion can be done easily as the surface of the sample can be easily patterned before anodization. This interdiffusion technique can be conveniently applied to the fabrication of nonabsorbing mirrors for high power laser application and to the fabrication of multiple wavelength lasers. Work is in progress to fabricate pulsed anodized ridge waveguide lasers with the area between ridges interdiffused by the anodic-oxide-induced interdiffusion. In this article, we will describe in detail the anodic-oxide-induced interdiffusion in GaAs/AlGaAs quantum structures.

The article is organized as below: in Sec. II, the sample structures, anodic-oxide-induced interdiffusion technique, and PL and transmission electron microscopy (TEM) measurements will be described; in Sec. III, the modeling of the results will be described; in Sec. IV, the results will be presented and discussed; and in Sec. V the article will be summarized.

II. SAMPLES AND EXPERIMENTS

Two structures (samples A and B) were grown by low pressure metal organic chemical vapor deposition (MOCVD) on p^+-GaAs substrates. The substrates were Zn doped to a carrier concentration of 1×10^{19} cm^{-3} and 2° off ⟨100⟩ towards ⟨110⟩. The layer structures for these samples are listed in Table I. All epilayers were nominally undoped.

After growth, the wafers are cleaved into 8 mm×8 mm pieces. Half of each piece was then covered with thermal glue. Each sample was rinsed in 10% HCl and deionized water, and nitrogen blow dried before it was picked up on the backside by a vacuum tweezers made by a stainless steel tube as shown in Fig. 1. The sample was then lowered to touch the electrolyte and then pulled up a little bit. The electrolyte consisted of ethylene glycol: deionized water: phosphoric acid (40:20:1 by volume). The anodic oxidation was performed at room temperature. The pulsed width was 1.0 ms, the total pulsed anodization time was 4 min. The pulsed anodization current density was in the range of 40–160 mA/cm^2 as determined by the leading edge of the pulse. The area covered with thermal glue was unanodized, while anodization takes place in the uncovered area to form a native oxide layer. When the pulse was on, anodization takes place, and when the pulse was off, the anodic oxide was etched slowly by the electrolyte. After anodization, samples were rinsed with deionized water, followed by acetone to remove the thermal glue, then by deionized water and N_2 blow dried. Each sample was then cleaved into two 4 mm×8 mm pieces, so that each piece has half the area anodized (4 mm×4 mm) and half the area unanodized (4 mm×4 mm). This enables a reasonable TEM and PL comparison between anodized and unanodized areas after interdiffusion process.

The interdiffusion was carried out in a RTA chamber with GaAs proximity cap in flowing argon ambient, the temperature ramp rate was 50 C/s.

A technique was developed to determine the Al profile of the quantum wells from the TEM images. The 90°-wedge TEM specimens are prepared by the cleavage method. Investigations of these specimens were performed in a Philips EM-430 transmission electron microscope operating at 300 kV. In this experiment, the specimens were orientated to the [100] zone axis and bright-field images were recorded using a CCD camera with a Gatan digital imaging software. Al profiles were determined by comparing the thickness fringes in experimental images with profiles calculated for different Al contents at 5% steps. This technique will be published elsewhere in detail.

Low temperature (12 K) PL measurements were performed on both the anodic oxidized and unoxidized sides of the samples. PL excitation was by an Argon ion laser (λ = 514.5 nm) modulated by a mechanical chopper. Excitation power was about 5 mW (cw). The detection system consisted of a 0.75 m grating spectrometer, silicon photodetector, and a lock-in amplifier referenced to the mechanical chopper. The PL spectra were acquired by a personal computer. A few samples were mounted together on the same cold finger in a cryostat, so that the PL intensity can be reasonably compared to each other. For anodized samples without RTA treatment,

the PL energies do not show significant shift from original as-grown sample.[30]

III. MODELLING OF THE INTERDIFFUSION AND EIGEN-STATES CALCULATION

In order to determine the interdiffusion parameters, such as diffusion coefficient and activation energy, from the experimental data, we first calculated the subband energies and wavefunctions in an interdiffusion modified single nonsquare quantum well,[4] and then compared the calculated interband transition energy to the PL data. The confinement profile of this interdiffused quantum well is nonlinear and was modeled here by an error function. The spatially dependent electron effective mass is taken into consideration using a nonparabolic band model derived from a fourth order expansion in k with the coefficients determined using a 14-band calculation, and excitonic effect was also considered.

The QW structure modelled here was an AlGaAs/GaAs single QW, which was nominally undoped in this study, and the effect of unintentional impurities was ignored. All the barriers in our samples were 50 nm, so that a finite thickness calculation was used.

The extent of the disordering process is generally characterized by a diffusion length L_d, defined here as $L_d=\sqrt{Dt}$,[37] where D and t are the Al–Ga interdiffusion coefficient and annealing time, respectively. In the model presented here, we have assumed an isotropic interdiffusion of Al and Ga with the diffusion coefficients being independent of their respective concentrations, which were also assumed to be equal and constant, i.e., we assumed Fick's second law of diffusion applies.[38] The diffused Al composition profile, $w(z)$, across the QW structure is given by[38]

$$w(z)=w_o\left\{1-\frac{1}{2}\left[\mathrm{erf}\left(\frac{L_z+2z}{4L_d}\right)+\mathrm{erf}\left(\frac{L_z-2z}{4L_d}\right)\right]\right\}, \quad (1)$$

where w_0 is the as-grown Al mole fraction in the barrier, L_z is the as-grown width of the QW, z is both the quantization and the growth axis (QW centered at $z=0$), and erf denotes the error function.[39] Equation (1) was used to obtain the interdiffusion induced QW parameters such as well depth, ΔE_r, which is defined as $\Delta E_r(z)=Qr[E_g(w_0)-E_g(z=0)]$, where $Eg(z)$ is the interdiffused bandgap [i.e., $E_g(z)=E_g[w(z)]$], Qr is the band offset splitting, and the subscript r denotes either the electron in the conduction band (C), heavy or light holes in the valence band (V=H or L). The interdiffusion induced QW confinement profile, $Ur(z)$, is defined by $Qr\Delta Er$. The numerical values of the above parameters are listed in Table II. The diffused QW subband edge ($k_\parallel=0$) at the zone center of Γ_6-valley symmetry can be calculated separately for the electron and holes, using the Ben–Daniel and Duke model[40] with a z position dependent effective mass on the interdiffused composition profile, by the one-dimensional Schrödinger-like equation, for the envelope function $\psi_{rl}(z)$, which is written as follows:

$$-\frac{h^2}{2}\frac{d}{dz}\left[\frac{1}{m^*_{\perp r}(z)}\frac{d\Psi_{rl}(z)}{dz}\right]+U_r(z)\Psi_{rl}(z)=E_{rl}\Psi_{rl}(z), \quad (2)$$

TABLE II. Parameters used in the calculation.

	$Al_wGa_{1-w}As$
Eg (eV)	$1.5194+1.36w+0.22w^2$ (for quantum well layer)
m_c/m_o	$0.0665+0.1006w+0.0137w^2$
m_{hh}/m_o	$0.34+0.16w$
m_{lh}/m_o	$0.0951+0.0441w+0.0097w^2$
$\varepsilon(x)/\varepsilon_o$	12.4-1.8w
$\alpha(x)$ (eV^{-1})	$0.0642+0.2733w$
$\beta(x)$ (eV^{-1})	$0.697+0.96w$
Q_c/Q_v	70:30

where $l=1,2,...$ are the QW subband levels for either the electrons (Cl) or holes (Vl), respectively; $m^*_{\perp r}(w(z))$ is the carrier effective mass in the z direction; $E_{rl}\equiv E_{rl}(k_\parallel=0)$ is the subband-edge energy, and the origin of the potential energy is taken at the bottom of the diffused QW. Equation (2) was solved numerically using a finite difference method with the corresponding confinement profile with a boundary condition taken to be zero at the end of a finitely high (energy) and thick ($\geqslant$50 nm) barrier.

The QW nonparabolic electron band-edge mass can be modelled by a fourth order expansion with the coefficients (α_0 and β_0) determined using a 14-band $\mathbf{k}\cdot\mathbf{p}$ calculation.[41] If we neglect the spin splitting term and keeping only a anisotropic fourth order term, the dispersion energy can be expressed as

$$E_c(k)=\alpha_0 k_z^4+\frac{h^2}{2m_c^*}(k_z^2+k_\parallel^2)+(2\alpha_o+\beta_o)k_z^2k_\parallel^2. \quad (3)$$

Two anisotropic QW masses in the confinement and in-plane directions can be derived and expressed as

$$m^*_{\perp c}(E_{cl},w)=\frac{m_c^*(w)}{2\alpha E_{cl}}\left[1-(1-4\alpha E_{cl})^{1/2}\right], \quad (4a)$$

and

$$m^*_{\parallel c}(E_{cl},w)=m_c^*(w)[1+(2\alpha+\beta)E_{cl}], \quad (4b)$$

respectively, $\alpha=\alpha(w)$ and $\beta=\beta(w)$ were linearly interpolated from data in Ref. 41; and $m_c^*(w)$ is the parabolic bulk effective mass; the numerical values of the above parameters are listed in Table II. It should be noted that the inequality, $m^*_{\parallel c}\geqslant m^*_{\perp c}$, holds for all well widths and, in the limit of large well widths ($L_z\to\infty$), the bulk effective mass is restored, i.e., $m^*_{\parallel c}=m^*_{\perp c}=m_c^*$.

The exciton wavefunction and binding energy can be obtained by knowing the solutions of Eq. (2) a priori. The 1S bound exciton wavefunction and binding energy (E_b) were determined by a perturbative-variational method.[42] Having the subbands in the interdiffused quantum well, the first electron-hole transition energy E_{11} can then be obtained from

$$E_{11}=E_g(z=0)+E_{vl}+E_{cl}-|E_b|. \quad (5)$$

The calculated quantum well interband exciton transition energies were fitted to the measured energy shift of PL peak by adjusting the value of D. The diffusion coefficient D can also be expressed by the Arrhenius relationship

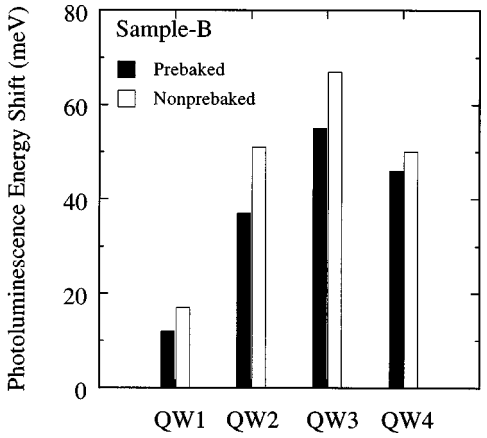

FIG. 2. Photoluminescence energy shift for anodized sample B annealed at 900 °C for 75 s. The anodization was done at 40 mA/cm^2 for 4 min. Solid bars represent the samples prebaked at 600 °C for 5 min.

$$D = D_0 e^{-E_A/kT}, \tag{6}$$

where D_0 is a prefactor, E_A is the activation energy, k is the Boltzmann constant, and T is the annealing temperature. D_0 and E_A were determined by a linear fit to the resulting values of $\ln(D)$ versus $1/kT$. The Al profiles for various quantum wells were also calculated by the Eq. (1) using the fitted value of D.

IV. RESULTS AND DISCUSSION

It is known[43] that GaAs oxide is thermodynamically unstable relative to the oxides of Ga and of As at typical processing temperatures. It is clear from our results that the anodically formed oxides are associated with the enhancement of group III interdiffusion. The interdiffusion results imply that the concentration of a native point defect, i.e., a group III vacancy or interstitial, is increased at elevated temperatures when annealing under an anodic oxide. For the impurity-free enhanced interdiffusion induced in GaAs by a deposited SiO_2 layer,[3] it is often assumed that an increased Ga vacancy concentration enhances the interdiffusion. However, the chemical interactions between GaAs and a hydrated mixture of Ga and As oxides are presumably quite different than those between GaAs and SiO_2.[29] Based upon previously reported measurements,[44] we predicted that the residual water in an anodically oxidized layer induces further oxidation of the GaAs at elevated temperatures.[30] We perform interdiffusion on two B samples under same conditions: anodized at current density of 40 mA/cm^2 for 4 min, rapid thermal annealed at 900 °C for 75 s together. The only difference is that one sample has been annealed (prebaked) at 600 °C for 5 min before the 900 °C rapid thermal annealing to reduce the concentration of residual water in the anodic oxide. The results are shown in Fig. 2. It is clearly seen that the residual water in the anodic oxide induces further interdiffusion, but it does not appear to be the main cause of the anodic-oxide-induced interdiffusion.

The diffusion coefficient, at an annealing temperature of 950 °C, of the group III species in QW1 of sample B was fitted to be 1.76×10^{-16} cm^2/s. The Al profile after 105 s annealing at 950 °C was computed using this coefficient and

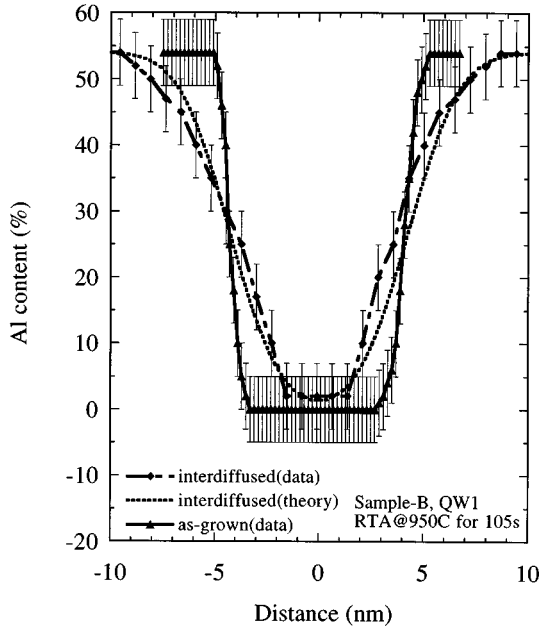

FIG. 3. Aluminum profile of the QW1 in the sample B (with anodization at 40 mA/cm^2 for 4 min) for as-grown and 105 s annealing at 950 °C. Theoretical calculated profile is also shown.

was also measured by TEM for comparison, as shown in Fig. 3. The Al profile for an as-grown sample determined by TEM is also shown for reference. As can be clearly seen in the figure, the Al composition has turned into a smooth profile after interdiffusion. This evidence shows the interdiffusion of the Al and Ga species, and because the theoretical and experimental data agree well, the diffusion was adequately described by a concentration independent coefficient. As a consequence of the interdiffused nonlinear profile, the subband energy will increase[4] and fundamental exciton transition should undergo a blue shift in energy.

Figure 4 shows PL spectra from sample A. The samples were annealed at 875, 900, 925, and 950 °C, the annealing time was 120 s. The upper part are the spectra from those unanodized areas, while the lower part are the spectra from the anodized areas. The unanodized quantum well is relatively thermally stable up to 925 °C, then it starts to show a strong blueshift at 950 °C. PL from anodized samples show continuous blue shift and significant intensity increase for annealing temperatures above 925 °C. This trend was observed for all samples anodized at different current densities. No linewidth broadening is observed from the PL spectra of the anodic-oxide-induced interdiffused samples. In Fig. 5, the PL peak energy shift of samples from sample A is plotted against annealing temperature for various anodization current densities. Also shown is the data for unanodized but annealed control samples of sample A as a control reference. The annealing time was 120 s. The variation in PL shifts in Fig. 5 was caused by experimental errors, presumably related to minor differences in oxide hydration and perhaps anneal temperature. The anodic oxide induced interdiffusion was not sensitive to the anodic current density in the range from 40 to 160 mA/cm^2 in the temperature range studied. This is due to the fact that the anodic oxide thickness is not sensitive

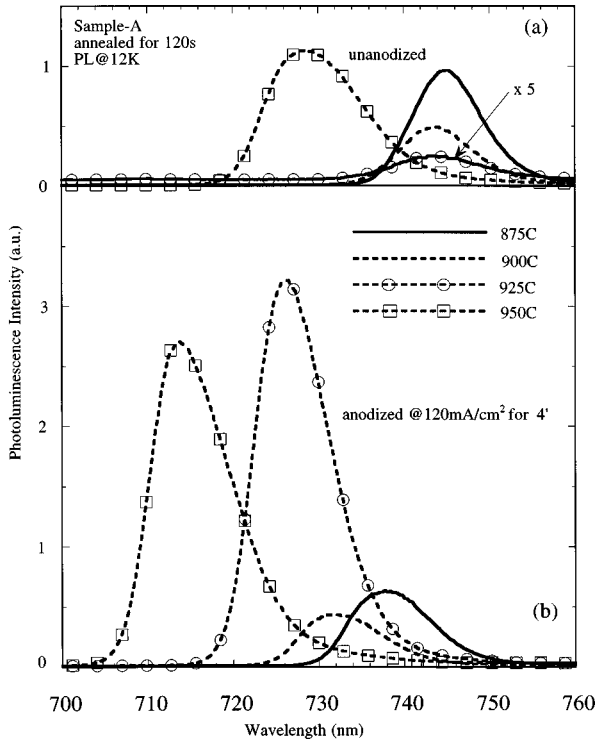

FIG. 4. Photoluminescence spectra at 12 K for sample A annealed at various temperatures for 120 s with (lower part) and without (upper part) anodic oxide. The anodization current density is 120 mA/cm^2 and the total anodization time is 4 min for all structures.

to the anodization current density at least in this current density range. The anodic oxide thickness' for examples of sample A anodized at 80, 160, and 200 mA/cm^2 for 4 min were determined to be 125, 110, and 125 nm, respectively. The diffusion coefficients D were determined by Eq. (1) and are plotted in Fig. 6 together with a fit for the 120 mA/cm^2 anodized sample. The data in Fig. 6 for the unanodized sample are not very reliable as the blue shift is very small

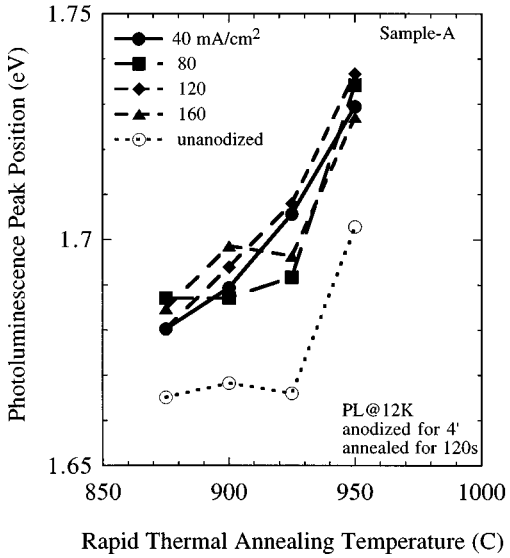

FIG. 5. Photoluminescence peak position as a function of rapid thermal annealing temperature for various anodic oxidization current densities. Lines are only shown to connect the experimental points.

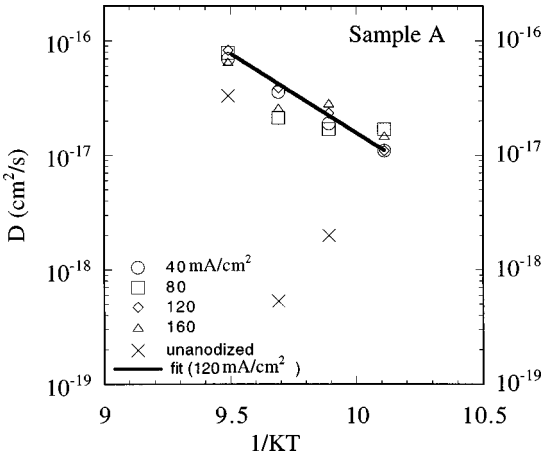

FIG. 6. D as a function of $(1/kT)$ for sample A annealed for 120 s. The experimental data for the anodized area were fitted for the samples anodized at 120 mA/cm^2 by the Arrhenius relationship with $E_A = 3.19$ eV and $Do = 1.12 \times 10^{-3}$ cm^2/s.

(except the 925 °C point). The diffusion coefficient for the anodized samples is somehow smaller than those obtained by SiO_2 impurity-free induced interdiffusion, but the activation energy is similar.[27,28]

In Fig. 7, we show the PL energy shift as a function of annealing temperature for sample B. The annealing time was 120 s. The relative PL shift used in this article is the PL energy difference between anodized area and unanodized area on the same piece of sample annealed together. The first and second quantum wells QW1 (8.6 nm) and QW2 (3.7 nm), as counted from the buffer layer, showed continuous blue shift. The thinnest and top quantum well, QW4 (1.3 nm), had strong blue shift even at 875 °C, and seems to saturate at 900 °C, and disappeared from the PL spectra above 900 °C. This is likely due to the fact that QW4 was so

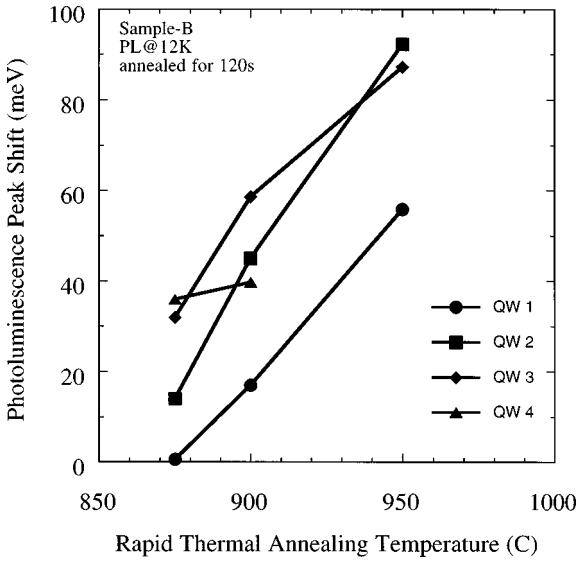

FIG. 7. Photoluminescence blue shift as a function of rapid thermal annealing temperature for each quantum well structure in sample B (4 quantum wells). The blue shift is the difference between PL energy of the anodized area and unanodized area. The anodization is performed at 120 mA/cm^2 for 4 min. The symbol represents the experimental data where the lines are only a guide to the eye.

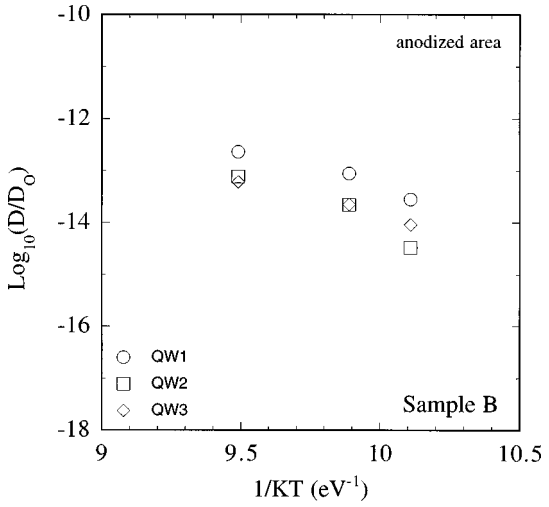

FIG. 8. Plot of $\log_{10}(D/Do)$ as a function of $(1/kT)$ for sample B annealed for 120 s. See the text for detailed description.

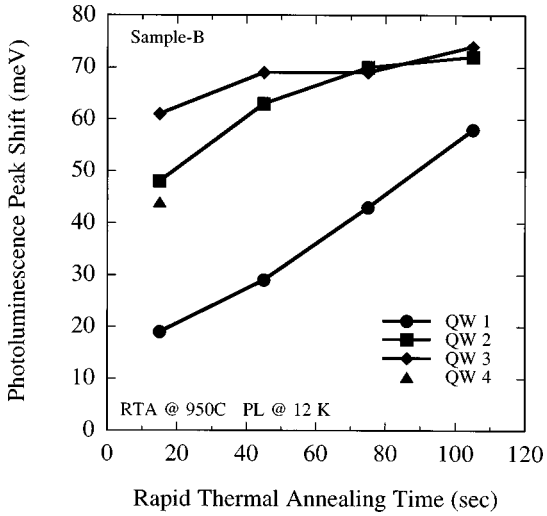

FIG. 9. Photoluminescence blue shift as a function of rapid thermal annealing time for anodized sample B. The blue shift is the difference between PL energy of the anodized area and unanodized area. The symbol represents the experimental data where the lines are only a guide to the eye.

thin and so close to the surface, it easily became very shallow and carrier confinement became very weak after anodization, and it finally became an indirect band gap material when enough Al atoms diffused from the indirect band gap material $Al_{0.54}Ga_{0.46}As$ barriers into the original GaAs well.

$\log_{10}(D/Do)$ versus $1/kT$ are plotted for the anodized area of QW1–3 in Fig. 8. The point defect concentrations in the epilayer are expected to vary substantially between the substrate and oxide interface at the beginning of an anneal. As with metals, it is expected that the point defect concentration profiles will flatten much faster than the measured atomic concentration profiles. Assuming that the point defect concentrations can be approximated as being close to their equilibrium concentrations, one may describe all of the results in terms of a single pair of values, Do and E_A. We have geometrically averaged the three slightly different values of Do associated with QW1–3 to obtain $Do=7.65\times10^{-4}$ cm^2/s. This value of Do was used to produce Fig. 8, which shows that $E_A=3.20\pm0.05$ eV applies to the observed interdiffusion. QW4 cannot be reliably compared with these because the PL for QW4 was not observed after annealing at temperatures above 900 °C. Although a nonequilibrium point defect concentration may have been caused by oxidation and/or RTA, the values of Do and E_A associated with Fig. 8 appear to be reasonably self-consistent and they are useful for prediction of D. The extent to which the point defect concentration has been affected by the original oxidation versus oxidation during RTA (via water in the oxide) remains to be determined. In Fig. 9, we plot the PL energy shift as a function of annealing time for these B samples. The annealing temperature was 950 °C. At this high annealing temperature, QW2 showed some saturation effect after being annealed for 45 s, QW3 showed clear saturation after annealed for 45 s. QW4 was only observed for annealing time of 15 s, and its blue shift was much lower than QW2 and QW3, indicating it might have reached saturation for shorter annealing time at this temperature. Only the thickest quantum well QW1 (8.6 nm) did not show signs of saturation.

V. CONCLUSIONS

In conclusion, we have reported a new method for the creation of interdiffused quantum wells. This technique is simple and inexpensive, and can be easily adopted in optoelectronic device fabrication. The anodic oxide thickness was insensitive to the currents in the experimental range we used. Water in the anodic oxides contributes to the interdiffusion, though it is not the main cause for interdiffusion. A saturation effect in the interdiffusion is observed for prolonged times for quantum wells of certain thickness. The calculated Al profile is compared to that determined from the TEM method. The activation energy is similar to those obtained from SiO_2 cap annealed quantum well structures.

ACKNOWLEDGMENTS

We thank Professor P. Zory, Dr. C. Largent, and J. S. O for fruitful discussion of pulsed anodization. We are grateful to Professor J. H. Marsh and Dr. A. M. Saher for helpful discussions. This work was partly supported by Australian Research Council and partly by RGC research grant of Hong Kong.

[1] *Quantum Well Intermixing for Photonics*, edited by E. H. Li (SPIE, Bellingham, MA, 1997).
[2] D. G. Deppe and H. Holonyak, Jr., J. Appl. Phys. **64**, R93 (1988).
[3] J. H. Marsh, Semicond. Sci. Technol. **8**, 1136 (1993).
[4] E. H. Li, B. L. Weiss, and K. S. Chan, Phys. Rev. B **46**, 15181 (1992).
[5] S. Yuan, N. Frank, G. Bauer, and M. Kriechbaum, Phys. Rev. B **50**, 5286 (1994).
[6] E. Kapon, N. G. Stoffel, E. A. Dobisz, and R. Bhat, Appl. Phys. Lett. **52**, 251 (1988).
[7] A. Wakatsuki, H. Iwamura, Y. Suzuki, T. Miyazawa, and O. Mikami, IEEE Photonics Technol. Lett. **3**, 905 (1991).
[8] T. Wolf, C. L. Shieh, R. Engelmann, K. Alavi, and J. Mantz, Appl. Phys. Lett. **55**, 1412 (1989).
[9] J. P. Moel, D. Melville, T. Jones, F. R. Shepherd, C. J. Miner, N. Puetz, K. Fox, P. J. Poole, Y. Feng, E. S. Koteles, S. Charbonneau, R. D. Goldberg, and I. V. Mitchell, Appl. Phys. Lett. **69**, 3516 (1996).
[10] Y. Nagai, K. Shigihara, S. Karakida, S. Karimoto, M. Otsubo, and K. Ikeda, IEEE J. Quantum Electron. **31**, 1364 (1995).

[11] E. C. Larkins, W. Benz, I. Esquivias, W. Rothemund, M. Bauemler, S. Weisser, A. Schonfelder, J. Fleissner, W. Jantz, J. Rosenzweig, and J. D. Ralston, IEEE Photonics Technol. Lett. **7**, 16 (1995).
[12] S. Burkner, J. D. Ralston, S. Weisser, J. Rosenzweig, E. C. Larkins, R. E. Sah, and J. Fleissner, IEEE Photonics Technol. Lett. **7**, 941 (1995).
[13] D. Hofstetter, H. P. Zappe, J. E. Epler, and P. Riel, Appl. Phys. Lett. **67**, 1978 (1995).
[14] B. S. Ooi, S. G. Ayling, A. C. Bryce, and J. H. Marsh, IEEE Photonics Technol. Lett. **7**, 944 (1995).
[15] S. Y. Hu, M. G. Peters, D. B. Young, A. C. Gossard, and L. A. Coldren, IEEE Photonics Technol. Lett. **7**, 712 (1995).
[16] N. Yamada and J. S. Harris, Jr., Appl. Phys. Lett. **60**, 2463 (1992).
[17] D. F. Welch, W. Streifer, R. L. Thornton, and T. Paoli, Electron. Lett. **23**, 525 (1987).
[18] A. McKee, C. J. McLean, G. Lullo, A. C. Bryce, R. M. De La Rue, J. H. Marsh, and C. C. Button, IEEE J. Quantum Electron. **33**, 45 (1997).
[19] A. Ramdane, P. Krauz, E. V. Rao, A. Hamoudi, A. Ougazzaden, D. Robein, A. Gloukhian, and M. Carre, IEEE Photonics Technol. Lett. **7**, 1016 (1995).
[20] S. R. Andrew, J. H. Marsh, M. C. Holland, and A. H. Ken, IEEE Photonics Technol. Lett. **4**, 426 (1992).
[21] S. F. Yu and E. H. Li, IEEE Photonics Technol. Lett. **8**, 482 (1996).
[22] A. S. W. Lee and E. H. Li, Appl. Phys. Lett. **69**, 3581 (1996).
[23] H. H. Tan, J. S. Williams, C. Jagadish, P. T. Burke, and M. Gal, Appl. Phys. Lett. **68**, 2401 (1996).
[24] H. H. Tan, J. S. Williams, C. Jagadish, P. T. Burke, and M. Gal, Mater. Res. Soc. Symp. Proc. **396**, 823 (1996).
[25] I. Harrison, H. P. Ho, B. Tuck, M. Henini, and O. H. Hughes, Semicond. Sci. Technol. **4**, 841 (1989).
[26] K. J. Beernink, R. L. Thornton, G. B. Anderson, and M. A. Emanual, Appl. Phys. Lett. **66**, 2522 (1995).
[27] S. Burkner, M. Maier, E. C. Larkins, W. Rothemound, E. P. O'Reilly, and J. D. Ralston, J. Electron. Mater. **24**, 805 (1995).
[28] I. Gontijo, T. Krauss, J. H. Marsh, and R. M. De La Rue, IEEE J. Quantum Electron. **30**, 1189 (1994).
[29] R. M. Cohen, Materials Science and Engineering: Report, Vol. 20, No. 4–5 (unpublished).
[30] S. Yuan, Y. Kim, C. Jagadish, P. T. Burke, M. Gal, J. Zou, D. Q. Cai, D. J. H. Cockayne, and R. M. Cohen, Appl. Phys. Lett. **70**, 1269 (1997).
[31] Y. Kim, S. Yuan, R. Leon, C. Jagadish, M. Gal, M. Johnston, M. Phillips, M. Stevens Kalceff, J. Zou, and D. Cockayne, J. Appl. Phys. **80**, 5014 (1996).
[32] M. J. Grove, D. A. Hudson, P. S. Zory, R. J. Dalby, C. M. Harding, and A. Rosenberg, J. Appl. Phys. **76**, 587 (1994).
[33] C. C. Largent, M. J. Grove, D. A. Hudson, P. S. Zory, and D. P. Bour, Solid-State Electron. **38**, 1839 (1995).
[34] C. H. Wu, P. S. Zory, and M. A. Emanual, IEEE Photonics Technol. Lett. **7**, 718 (1995).
[35] S. Yuan, G. Li, H. H. Tan, F. Karouta, and C. Jagadish, IEEE/LEOS '96 Proceedings, 1996 (unpublished), Vol. 2, p. 132.
[36] M. A. Emanuel, N. W. Carlson, and J. A. Skidmore, IEEE Photonics Technol. Lett. **8**, 1291 (1996).
[37] It should be noted here that the definition of L_d varies in the literature; for instance, some authors define L_d as $2\sqrt{Dt}$, see K. Kash *et al.*, J. Appl. Phys. **63**, 190 (1988). But the factor of 2 is present in Eq. (1).
[38] J. Crank, in *The Mathematics of Diffusion*, 2nd ed. (Oxford University, Oxford, 1975), p. 15.
[39] M. Abramowitz and I. A. Stegun, *Handbook of Mathematical Functions* (National Bureau of Standards, Washington, DC, 1964).
[40] D. J. BenDaniel and C. B. Duke, Phys. Rev. **152**, 683 (1966).
[41] U. Ekenberg, Phys. Rev. B **40**, 7714 (1989).
[42] E. H. Li and B. L. Weiss, Proc. SPIE **1675**, 98 (1992).
[43] C. D. Thurmond, G. P. Schwartz, G. W. Kammlott, and B. Schwartz, J. Electrochem. Soc. **127**, 1366 (1980).
[44] S. P. Murarka, Appl. Phys. Lett. **26**, 180 (1975).